Available online at www.sciencedirect.com

ScienceDirect

Advances in Space Research 74 (2024) 3081–3100

ADVANCES IN SPACE RESEARCH
(a COSPAR publication)

www.elsevier.com/locate/asr

Onboard guidance and control algorithms for increased autonomous aerobraking capabilities at Mars

Alban Beshaj, Alessandro Morselli *

Politecnico di Milano, Dept. Aerospace Science and Technology, Via La Masa 34, 20156, Milan, Italy

Received 22 December 2023; received in revised form 26 April 2024; accepted 8 July 2024
Available online 15 July 2024

Abstract

Aerobraking represents a valuable option for interplanetary missions thanks to its capability of reducing the orbital semi-major axis through multiple atmospheric passages, thus with limited fuel consumption. However, due to structural and thermal loads the spacecraft undergoes, mission risks and ground operations costs increase. This study aims to tackle this aerobraking drawback by enhancing its autonomy. The main activities required for aerobraking execution, including atmospheric prediction, orbital state estimation, and orbit control, are tailored for onboard execution. Regarding orbit control, two different methodologies, differentiated by working principle and prediction horizon breadth, are investigated. The first plans orbit control manoeuvres based on the prediction of the atmospheric conditions for a single upcoming pericentre, while the second schedules and optimizes the manoeuvres considering the recent atmospheric conditions experienced by the spacecraft and the altitude trend of multiple upcoming pericentres. The whole operational concept is tested within a simulated environment, with the primary objective of accurately reproducing the intense atmospheric variations of the Martian atmosphere, which represents the most challenging aspect during aerobraking execution. The numerical testing, involving the simulation of different aerobraking regimes under varied conditions, shows that the natural dynamics of the orbital motion can be exploited to minimize both fuel consumption for orbit control manoeuvres and spacecraft load variations, thus enabling more efficient aerobraking and more stable flight conditions, even with the limited predictive capabilities that characterize onboard resources. Both control logics permit the aerobraking execution without exceeding the maximum allowed thermal limits, hence showing their effectiveness. Furthermore, a Monte Carlo analysis conducted on a complete aerobraking simulation reveals a 25.5% reduction in propellant consumption and a 9.4% reduction in heat rate variability when the orbit control decision process uses information relative to multiple future pericentres.

Keywords: Autonomous aerobraking; Trajectory control; Mars

1. Introduction

In recent years, the increased complexity of interplanetary missions, driven by the advancement of mission objectives, has led to the demand for more massive payloads. Due to the high energy required for interplanetary transfers, it has become necessary to investigate strategies for improving transfer efficiency with the goal of raising the payload-to-mass ratio.

Besides being of great scientific interest, the atmosphere plays a paramount role in transfer efficiency enhancement. It can be exploited in different phases of the mission (Walberg, 1985). The first context concerns the initial approach to the planetary system of interest. After the interplanetary leg, energy is required to insert the spacecraft into the planetary system, i.e., to transition from the deep-space hyperbolic trajectory to a close orbit around the main body. The impulse required to fill the energy

* Corresponding author.
E-mail addresses: alban.beshaj@polimi.it (A. Beshaj), alessandro.morselli@polimi.it (A. Morselli).

https://doi.org/10.1016/j.asr.2024.07.021
0273-1177/© 2024 COSPAR. Published by Elsevier B.V.

gap between the two trajectories can be provided by the propulsion subsystem (with propellant consumption) or by exploiting the atmospheric drag generated from the passage through the planetary atmosphere. The associated aero-assisted manoeuvre is called aerocapture, and it is capable of providing significant propellant savings with a single deep atmospheric passage. However, the large amount of delta-v delivered comes at the expense of high mission risks related to the significant thermal and structural loads the satellite undergoes and the risk of impact with the planet surface. These aspects underlie the low maturity of aerocapture that requires further studies, experiments, and validations before being adopted in real missions (Spilker et al., 2019).

The second context in which the atmosphere can be exploited to reduce propellant consumption concerns the phase after the Orbit Insertion manoeuvre (OIM). Typically, post-OIM orbits are characterized by high eccentricities, and additional manoeuvres are required to reach the science orbits which are usually located at lower altitudes. Although this transfer might include one or more changes of orbital plane, the primary purpose of the manoeuvres is to reduce the orbital semi-major axis. The aerobraking is an aero-assisted manoeuvre that gradually dissipates orbital energy through multiple controlled atmospheric passages, enabling the achievement of the science orbit with reduced propellant consumption. A key difference with respect to aerocapture concerns the depth of atmospheric passages. Since the impulse required by the aerobraking gradual energy dissipation is contained, these passages occur at higher altitudes. This aspect results in the advantage of reduced thermal and structural spacecraft loads. The first planetary mission to attempt an aerobraking was the Magellan mission in 1993 (Lyons et al., 1995). Its successful execution, combined with the fact that it was not considered in the mission design, increased the aerobraking appeal. In the following years, it was performed during NASA's Mars Global Survey (MGS) (Lyons et al., 1999), Mars Odyssey (Smith and Bell, 2005), and Mars Reconnaissance Orbiter (MRO) (Zurek and Smrekar, 2007) missions. In 2014 and 2017, ESA operated aerobraking in the Venusian and Martian context for Venus Express (VEX) (Val Serra et al., 2011) and ExoMars (Castellini et al., 2019) missions. The successful execution of aerobraking during these missions demonstrated the manoeuvre effectiveness, leading to its last execution during the MAVEN mission (Demcak et al., 2020) and to its consideration for the future EnVision mission (de Oliveira et al., 2018).

Despite the propellant savings, aerobraking revealed several drawbacks since its initial applications (Spencer and Tolson, 2007). The thermal and structural loads and cycles associated with the multiple passages through the atmosphere can jeopardize mission success, thus regular supervision is required to ensure mission safety. Ground personnel must react promptly to unexpected variations in the environment conditions through intensive operations, especially during the last phase, when atmospheric passages are much more frequent. It is important to note that, as aerobraking is executed close to the structural and thermal limits of the spacecraft to rapidly achieve the science orbit, atmospheric variabilities can lead to loads exceeding the spacecraft limits, potentially resulting in mission failure. This problem is even more pronounced in the Martian context, where the thin and rarefied atmosphere is more susceptible to contingent radiative conditions. Furthermore, Martian topography induces the propagation of gravitational and longitudinal waves that enhance the instability of the external atmospheric layers (Moudden and Forbes, 2008), which are relevant for the aerobraking execution. In addition, the light-time delay might be high if aerobraking is performed at great distances (e.g., Titan).

Therefore, the main limitation of current aerobraking strategies lies in the operational burden it places on the ground segment, which constitutes one of the main cost items of the manoeuvre. To address this issue, several studies have focused on enhancing aerobraking autonomy. The first improvement that contributed significantly in this context is the Pericenter Time Estimator (PTE). It is an algorithm developed and tested in background during Mars Odyssey mission (Johnson and Willcockson, 2003), with the purpose of automating some of the aerobraking activities by means of a temporal shifting of uploaded commands required to compensate for the orbital period decrement. The PTE proved to be a reliable solution during MRO mission (Long et al., 2008), and its success led to the utilization of the tool in more recent aerobraking.

In addition to in-flight adopted solutions, several research studies have been conducted to tackle the operational cost issue, focusing on enhancing autonomy in the various activities required to perform aerobraking. Both heuristic strategies (Maddock et al., 2012) and deep reinforcement learning approaches (Falcone and Putnam, 2023) have been investigated to accomplish the orbit control task, which is paramount for the containment of spacecraft loads. In most control approaches, orbit control action is based on the prediction of surrogate variables of the real spacecraft limits, such as heat rate, heat load, and dynamic pressure. Prince et al. (2009) proposes the direct consideration of the temperature of a specific satellite component as an alternative to the conservative surrogate variables approach. Although this solution can yield to optimized aerobraking, i.e., faster execution of the manoeuvre, it adds complexity to the control decision-making process and affects operations flexibility. Other studies have examined the possibility of using solar panels rotation during the atmospheric passage to augment the control authority (Falcone and Putnam, 2019). Besides being functional to time and fuel consumption reduction of the aerobraking campaign, this interesting approach could be used to counteract atmospheric variabilities, damping the unpredicted loads experienced by the spacecraft. However, the rotation of the solar panels in presence of aerodynamic forces impacts the mass of the actuators responsible for the rotation. Therefore, trade-off analyses and additional test campaigns are required to assess the effectiveness of that solution.

Besides on-board autonomy, for an improved aerobraking strategy it is also paramount to properly predict and model the atmosphere of the planet. Considerable research work has been also devoted to the characterization of the Martian atmospheric dynamics (Moudden and Forbes, 2010; Liu et al., 2017). Understanding the atmospheric condition evolution is crucial because it constitutes the main source of uncertainties affecting the loads the spacecraft undergoes, and an accurate prediction of atmospheric relevant parameters can mitigate the risks associated with aerobraking. Several models of variable complexity have been developed to accomplish the prediction task, ranging from sophisticated models that embed wave structures propagating through the atmosphere (Moudden and Forbes, 2015) to simpler exponential models (Tolson and Prince, 2011). While the former category can provide more accurate predictions, exponential models have been preferred in the mission operational framework since the lack of frequent atmospheric measurements, particularly pronounced in the first phases of the aerobraking campaign, affects the calibration of complex models.

The past passages information required for the prediction activity is collected using accelerometers, a fundamental sensor both in aerobraking operations and also crucial for what concerns spacecraft navigation (Tolson et al., 1999; Tolson et al., 2005; Tolson et al., 2008). Several research works have focused on leveraging accelerometer data to relieve the need for radiometric navigation, which involves the expensive resources of deep-space antennas. In Jones et al. (2015), telemetry is used in the determination process performed through batch filtering, while Jah et al. (2008) proposes an alternative approach that involves processing accelerometer data as external measurements in a sequential filter. As reported in Han and Young (2019), the first method exhibited poor convergence with real-world errors, while the second is incompatible with the traditional orbit determination processes. Consequently, the approach developed in Young (2018), which consists of using accumulated accelerometer data values as observables, has been considered for MAVEN aerobraking. An alternative approach proposed in Hanna and Tolson (2002) consists of reconstructing the orbital trajectory through propagation, considering a low-order gravity field and atmospheric drag in the dynamical model. The authors support the suitability of the method by leveraging on the fact that precise orbital state knowledge, crucial for science purposes, is not strictly required by aerobraking execution.

The operational framework implemented in this work avoids filtering techniques favoring the orbital state reconstruction through on-board propagation. Taking into account the relevant orbital perturbations of the Martian environment, this approach can provide a stable estimation of pericentre altitude, which is the relevant control parameter in aerobraking orbital control. The orbit control is performed through two different heuristic strategies that are analysed and compared. The first one is based on the prediction of the upcoming single passage atmospheric condition, while the second determines the control action according to the pericentre trend of multiple upcoming atmospheric passages, retrieved through on-board propagation. The prediction of the relevant atmospheric parameters is obtained through a simple tunable exponential model, whose free parameters are set using the data collected by the on-board accelerometer during past passages. The operational loop implemented is numerically tested in a simulated environment that accurately reproduces the atmospheric dynamics utilizing the Martian Climate Database (MCD). The development of this flexible and robust simulation environment, which enables the testing of autonomous aerobraking operational frameworks on different Martian regions, combined with the integration of the natural orbital dynamics in the aerobraking orbit control, constitute the main contributions of this work. Furthermore, through the testing under different regimes and non-nominal conditions, the study demonstrates how considering the multiple pericentre altitude trends in control manoeuvres scheduling and optimization is beneficial in terms of fuel consumption and stability of flight conditions.

The remainder of this paper is organized as follows. Section 2 provides an overview of the aerobraking phases, the theoretical framework used in the study, and the details of the reference mission considered. Section 3 highlights the methodology and the assumptions which underlie the work development. In Section 4, the onboard operations required for aerobraking execution are presented, and in Section 5, the results of their testing and the relative considerations are reported. Finally, Section 6 draws the conclusions and possible further developments of the work.

2. Background and definitions

From an operational point of view, aerobraking can be divided into the following sub-phases (Lyons et al., 1995):

Walk-in represents the phase where contact with the atmosphere is established. The pericentre altitude is gradually lowered to reach the aerobraking regime condition.

Main phase denotes the period in which significant dissipation of orbital energy occurs. It is the most extended aerobraking phase.

End game differs from the main phase for the longer atmospheric passages, which result in an increased heat load experienced by the spacecraft. This phase starts when the orbital period drops below 6 h, hence multiple passes are performed each day. In addition, interruptions in communications with ground are more frequent (Denis et al., 2018).

Walk-out represents the last phase of aerobraking. The pericentre is raised, enabling the satellite insertion into the science orbit.

Fig. 1 provides a simplified representation of the trajectory evolution during each aerobraking phase, along with the trend of the most relevant parameters.

This work will focus on the autonomous execution of the main phase and the end game. Due to their prolonged duration, these two phases are the main contributors to the operational effort required to perform aerobraking.

The typical orbit control strategies of the main phase and end game are based on the definition of a control corridor, expressed in terms of surrogate variables of the true spacecraft thermal and structural limits, such as heat rate, heat load, and dynamic pressure. A time constraint provides the lower bound of the corridor, as the phase duration must be limited to reduce the costs associated with the operations. The upper bound is straightforwardly set by the spacecraft withstanding capabilities; the structure loads must be contained to guarantee mission safety during the aerobraking execution. Once the corridor is defined, the control action is performed to maintain the control variable inside the bounds through Orbit Control Manoeuvres (OCMs), which consist of apocentre burns to adjust the pericentre altitude, as illustrated in Fig. 2. According to the predicted atmospheric conditions, the pericentre altitude can be raised to encounter less dense atmospheric layers in case of upper bound violation or decreased if the lower constraint is not fulfilled.

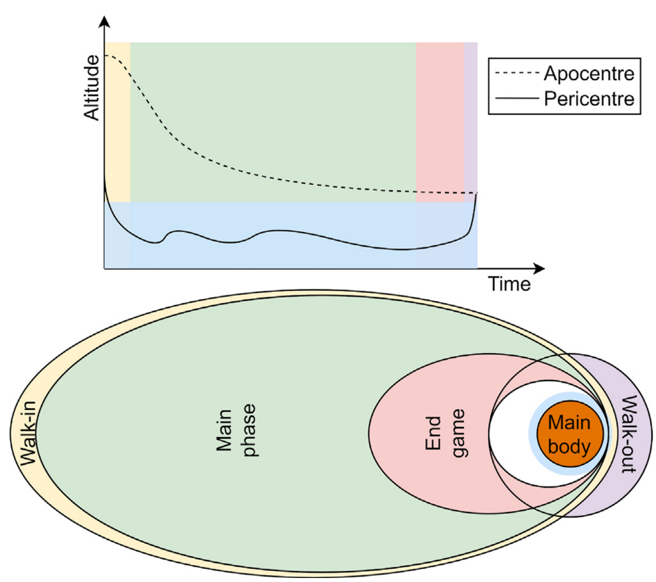

Fig. 1. Conceptual representation of trajectory, pericentre, and apocentre altitude evolution during aerobraking phases.

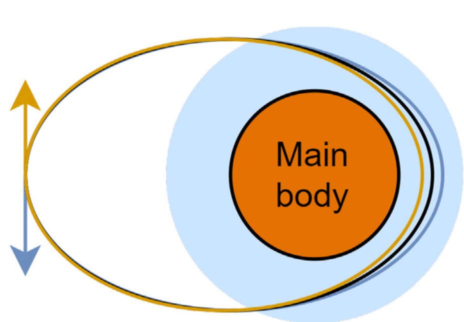

Fig. 2. Representation of OCMs. The manoeuvre in gold represents a pericentre decrease manoeuvre, while the blue one is a pericentre increase manoeuvre. The black curve is the orbit with no manoeuvre.

2.1. Reference frames

The reference frames used within the study framework are the following:

J2000 It is an inertial reference frame defined by the terrestrial equator and vernal equinox at the J2000 epoch. In this work, its origin is set at the centre of mass of Mars, and it is used for the equation of motion propagation.

Radial Tangential Normal (RTN) This is a non-inertial reference frame centered in the main body, defined by the vector pointing from the main body centre of gravity to the satellite, the orbit tangential direction, and the orbital angular momentum vector. RTN is used in the execution of OCMs, which consist of tangential burns.

Mars-Centered Mars-Fixed(MCMF) It is a non-inertial reference frame centered on Mars. Its axis are defined by Mars' prime meridian and the planet's rotational axis. Within the context of this work, this reference frame is introduced to determine quantities associated with planetodetic coordinates, such as atmospheric density and perturbations related to gravitational anomalies. The model proposed in Konopliv et al. (2006) is used for the Mars rotational dynamics evolution, and given the specific gravitational model used in this work, the rotational model parameters are taken from Konopliv et al. (2016).

2.2. Equations of motion

The orbital motion is modelled using Cowell's formulation (Vallado, 2001). The resulting equations of motion are provided below:

$$\ddot{\boldsymbol{r}} = -\frac{\mu}{r^3}\boldsymbol{r} + \boldsymbol{a}_p \tag{1}$$

Where μ represents the planetary gravitational parameter and $\boldsymbol{r}$ is the spacecraft's position with respect to the main body. The term $\boldsymbol{a}_p$ incorporates the additional forces that affect the orbital motion beyond the primary gravitational attraction.

In the context of aerobraking, the wide eccentricity range of the orbits and the resulting variation in altitudes during the motion beg for the consideration of several perturbations. As reported in Fig. 3, where the magnitudes of the most relevant perturbation are represented as a function of the altitude above the Martian mean radius, different flight regions are characterized by different dominant perturbations. Specifically, atmospheric drag acceleration, here obtained using an exponential model, significantly impacts the motion for altitudes below 150 km. Among the perturbing bodies, the dominant contribution is given by the Sun, followed by Jupiter and Earth. Phobos and Deimos provide a non-negligible contribution, especially for those orbital regimes for which close encounters or resonances could occur. Furthermore, the first spherical harmonics represent the dominant perturbation for a wide range of altitudes. Therefore, to accurately simulate the orbital motion during aerobraking execution, the aforementioned perturbations must be considered in the numerical propagation of the reference solution.

2.3. Reference mission

The reference aerobraking campaign of this work is the one performed by TGO (Castellini et al., 2019), which started on 14 March 2017 and was completed after 11 months, with an interruption of 2 months due to a solar conjunction. TGO started aerobraking from a 74° inclination orbit with an orbital period of 24 h, and thanks to the gradual energy dissipation resulting from the atmospheric passages, it was reduced to approximately 2 h.

The most relevant physical parameters of TGO in its aerobraking configuration used in this work are reported in Table 1:

2.4. Accelerometer measurements

The versatility of accelerometers has fostered their use in space missions, making them even more crucial for aerobraking missions as they represent the foundation of autonomy enhancement. Within this context, these sensors can be employed to characterize the atmospheric dynamics and to limit the time allocated to tracking and navigation. In the simulations conducted in this work, the model described in Rogers (2003) is considered in order to provide more realistic measurements. Accelerometer data $\boldsymbol{a}_{meas}$ are generated from the ideal drag acceleration $\boldsymbol{a}_{ideal}$ through the following expression:

$$\boldsymbol{a}_{meas} = \boldsymbol{A}\,\boldsymbol{a}_{ideal} + \boldsymbol{a}_{bias} + \boldsymbol{a}_{noise} \tag{2}$$

where $\boldsymbol{A}$ is a 3x3 matrix with the diagonal terms representing the sensor scaling factors and the extra-diagonal terms associated with the misalignment errors, $\boldsymbol{a}_{bias}$ is the bias, and $\boldsymbol{a}_{noise}$ represents the noise.

During flight operations, the accelerometer is calibrated for every passage by processing the data prior to the atmospheric entry and successive to the atmospheric exit (Tolson et al., 2008). For the purposes of this work, the processing routines of the bias estimation are not considered, and following the approach of Jones et al. (2015), a constant bias value is assumed.

Table 1
TGO parameters in aerobraking configuration.

Parameter	Symbol	Value	Unit
Mass	m	1750	kg
Solar panels area	A_P	22	m^2
Total front area	A_F	29.3	m^2
Ballistic coefficient	B	60	kg/m^2
Maximum heat rate	$\dot{q}_{\max}$	0.28	W/cm^2
Maximum heat load	$Q_{\max}$	50	J/cm^2
Starting orbital period	T_0	24	$hours$
Exiting orbital period	T_f	2	$hours$

3. Methodology

The objective of this work is to assess whether it is possible, leveraging on the information directly available onboard the spacecraft, to autonomously optimize

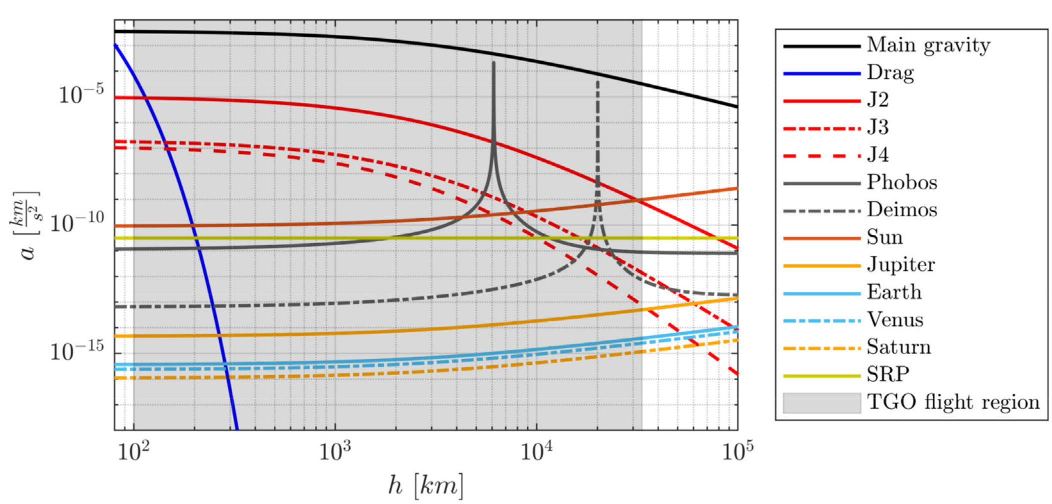

Fig. 3. Magnitude of the main orbital perturbation accelerations as a function of the altitude above Martian mean radius. Phobos and Deimos contributions curves represent their maximum contribution, hence their potential effect during close approaches.

onboard the propellant used for OCMs and reduce spacecraft heat rate variability during aerobraking execution by exploiting natural orbital dynamics. In order to verify if the implemented solutions achieve this objective, their testing in a relevant simulation environment is required. This testing involves the simulation of the autonomous operations framework in which the control logics are integrated and the actual environment where they are supposed to be used. Therefore, the adopted approach consists of two components. The first one consists in implementing and executing on-board routines that allow to guide and control the spacecraft during aerobraking. The second one is instead the simulation layer, which reproduces the real environment and provides the actual trajectory (the ground truth) and the atmospheric drag experienced during the pericentre passage. This section, after introducing the motivations and assumptions behind the proposed simulation approach, outlines the real world models (characterized by a higher complexity level) and the on-board models (used within the proposed algorithms for propagation and estimation). Finally, the approach used for the initialization of the simulations is outlined.

3.1. Motivations and assumptions

Given the risks associated with aerobraking, a realistic reproduction of the environmental characteristic is paramount to provide meaningful results. In the Martian context, the most peculiar feature is represented by the atmosphere, which, with its high variability, amplifies the risks and becomes a driving element in the control logics design. Based on this consideration and the level of automation already achieved in attitude control through the use of reaction control system and reaction wheel actuators and star tracker sensors, a 3-degree-of-freedom simulation approach has been preferred. Although the couplings between translation and rotational motion may be relevant, the focus on the translational motion is justified by the preliminary nature of this work and by the purpose of testing the orbit control strategies, which are primarily affected by atmospheric instability.

The selected simulation approach is based on a set of simplifying assumptions that are all encompassed by the more general assumption of perfect attitude knowledge. First, OCMs are considered to be performed in an ideal purely tangential direction, hence no off-pointing is taken into account in this study. Secondly, the accelerations experienced by the spacecraft and other vectorial quantities are provided in the J2000 reference frame. For instance, the generation of accelerometer measurements realized through Eq. (2) is performed directly in the inertial reference frame. Furthermore, due to the absence of the attitude dynamics, no rotational contributions are considered in the acceleration detected by the accelerometer. As done for the bias, this last effect is reconstructed onboard via IMU measurements during flight operations (Tolson et al., 1999). Although the mismodeling resulting from these simplifications is partially absorbed by the discrepancies between the onboard and real world models, the limitations of the assumptions made have to be assessed in further developments.

3.2. Real world models

The real-world models are the set of dynamical models representing the actual environment. As shown in Fig. 3, several perturbations are relevant for the accurate orbital motion description. Given the significant impact of the atmospheric drag, and more specifically of the atmospheric variabilities, the focus is placed on the modelling of this environmental feature. For the other perturbations, a reasonable trade-off between model refinement and simulation times has been applied. Mars gravitational anomalies are approximated by a non-spherical potential function. Specifically, the gravity field is reproduced through a 20x20 expansion of the MRO120D gravitational model (Konopliv et al., 2016), which provides satisfactory accuracy for aerobraking simulation purposes. Concerning the perturbing third bodies, their influence strongly depends on the bodies' configuration and, consequently, on the simulation epoch. Given the reference aerobraking mission, the Sun, Jupiter, Earth, Phobos, and Deimos perturbing effects are considered relevant. Their position is obtained from the SPICE kernels `de425s.bsp` and `mar097s.bsp`, which respectively contain the ephemeris of the external bodies and the bodies belonging to the Martian planetary system. The cannonball model is used for SRP perturbation, and the shadow function is determined according to the bi-conical shadow model (Montenbruck and Gill, 2000). The solar panels area reported in Table 1 is used as the reference surface due to its significant size on TGO spacecraft, and the relative reflectivity coefficient provided in Montenbruck and Gill (2000) is considered. For the drag perturbation, the area exposed to the aerodynamic flow is the total front area of the spacecraft in Table 1. Given that during aerobraking the rarefied outermost atmospheric layers are involved, a constant drag coefficient (C_D) of 2.2 is assumed, and no lift forces are considered.

Atmospheric drag is strictly related to mission safety through the loads that it exerts on the structure. Therefore, accurately reproducing the expected atmospheric variations is paramount for this study. For this purpose, the MCD is used. It is a database containing the physical and chemical properties of the Martian atmosphere. The data are generated by numerical simulation of Global Circulation Models (GCMs) (Forget et al., 1999), which are complex models that attempt to simulate atmospheric dynamics considering the phenomenology of the Martian environment. In the simulation performed in this study, the climatology scenario `clim_aveEUV`, which represents the atmospheric conditions of a standard Martian year, is considered. The MCD is used in its high-resolution mode, meaning that the atmospheric properties are based on the high-precision topography model MOLA 32. Small and large-scale atmospheric perturbations are considered, with a default vertical wavelength of 16,000 meters for the former. Finally, the trajectory propagator provides all the other inputs required by the MCD. Additional information about these inputs and the tool's settings can be found in Millour et al. (2017).

According to the previous missions that performed aerobraking in the Martian environment, the control variable selected for this study is the heat rate peak experienced during the atmospheric passage. Since accurate thermal modeling goes beyond the purposes of the work, the following heat rate indicator is used in the simulations:

$$\dot{q} = \frac{1}{2}\ \rho\ v_{rel}^3 \tag{3}$$

Where ρ is the atmospheric density provided by the MCD and v_{rel} is the spacecraft relative velocity with respect to the atmosphere, retrieved from the propagated trajectory and the rotational model of the planet. Given its greater relevance compared to the minor and more predictable radiative heat, only the convective contribution is considered. Indeed, the convective heat rate underlies the challenges of aerobraking orbital control due to its proportionality with the highly variable atmospheric density.

3.3. Onboard models

The dynamical models discussed in the previous section, which constitute the real-world model, are also employed onboard in the aerobraking operational loop. However, due to the limited onboard resources, there are some differences in the fidelity of these models. Specifically, the onboard gravitational model is a 4x4 expansion of MRO120D to enhance the computational efficiency in propagation. The atmosphere is modeled through an exponential model. The relative density-altitude relation is provided by:

$$\rho(h) = \rho_0 \exp\left(-\frac{h - h_0}{H}\right) \tag{4}$$

where ρ_0 and h_0 are the reference density and reference altitude, respectively, and H is the scale height.

The same heat rate indicator defined in Eq. (3) is used onboard by the orbital control routines. Differently from the real world one, in this case, it is computed using the density provided by the onboard exponential model and the relative velocity retrieved from the onboard propagator.

3.4. Simulation initialization

Focusing on the main phase and end game, in this work, the modelling of the walk-in is considered secondary. The absence of this phase begs for a simulation initialization that provides the data relative to the first atmospheric passages, which are required for the initialization of the onboard operations. Furthermore, for the testing purposes detailed in Section 5, the simulation initialization is required to collocate the pericentre in specific regions of the Martian atmosphere. To fulfil these functions, starting from the orbital period T, orbital inclination i, latitude ϕ and longitude λ of the pericentre in the MCMF, and the target heat rate $\dot{q}_{target}$ the simulation initialization fixes the aerobraking starting orbit through the following steps. Firstly, assuming an unperturbed Keplerian motion, the semi-major axis a is obtained from the orbital period:

$$a = \sqrt[3]{\mu\left(\frac{T}{2\pi}\right)^2} \tag{5}$$

To fully define the orbital shape, the eccentricity is computed finding the zero of the difference function between the pericentre heat rate $\dot{q}$ and the target one $\dot{q}_{target}$:

$$f(e) = \underbrace{\frac{1}{2}\ \rho(e)\ v_{rel}^3(e)}_{\dot{q}(e)} - \dot{q}_{target} \tag{6}$$

Where the density ρ is provided by the MCD at the pericentre altitude relative to the values of a and e, and v_{rel} represents the spacecraft's relative velocity with respect to the atmosphere at the pericentre. By neglecting the atmospheric velocity, v_{rel} can be expressed as a function of a and e through the following equation:

$$v_{rel} = \sqrt{\frac{\mu}{a(1-e^2)}}(1+e) \tag{7}$$

Finally, the pericentre state is fully characterized through a root-finding problem, which provides the pericentre velocity vector that satisfies the constraints relative to the inclination provided in input and shape parameters already fixed. A backward propagation to the first past apocentre and a forward one for a specific number of atmospheric passages is performed to collect the data required by the initialization of the onboard operations.

4. Autonomous onboard operations

4.1. Atmospheric prediction

The prediction of the atmospheric conditions is critical in the orbit control process. OCMs are planned and executed based on the predicted peak density and the relative spacecraft load. Several models of varying complexity can be employed to carry out the prediction task. During TGO aerobraking, GCMs and exponential models have been used. However, given the similar results achieved by the different models, the latter has been preferred in most of aerobraking phases for its simplicity (Castellini et al., 2019). The flexibility enhancement that characterizes the exponential model has led to its use in the autonomous operational framework of this work.

Throughout aerobraking execution, the pericentre flight region changes over time due to the orbit evolution, fostering the variability of the encountered atmospheric conditions. One key factor influencing the atmospheric density in a specific region is the illumination condition. As illustrated in Fig. 4, according to the Sun's longitude in the MCMF frame, and consequently to the pericentre local time, the atmospheric layers can expand or contract, considerably altering the density values. Therefore, it is crucial to account for this aspect in the exponential model presented in Subsection 3.3. As shown in Tolson and Prince (2011), this can be achieved by embedding the recently experienced densities into the model. The resulting tunable exponential model is represented by the following relation in its logarithmic form:

$$\log \rho(h) = a + b\left(h - h_p\right) \tag{8}$$

where H is the scale height, $a = \log\left(\rho_p\right)$ and $b = -\frac{1}{H}$. The density ρ_p and altitude h_p represent the reference values that, for the aerobraking context, are considered equal to the pericentre density and altitude respectively.

After the passage, the parameters a and b relative to the past passage can be fixed using the collected density data that can be retrieved from the accelerometer measurements through the following relation:

$$\rho = \frac{2\ a_{meas}\ m}{v_{rel}^2\ C_D\ A} \tag{9}$$

where a_{meas} is the measured acceleration magnitude, C_D is the drag coefficient, A is the cross area exposed to the aerodynamic flow, m is the satellite's mass, and v_{rel} is the relative velocity of the spacecraft with respect to the atmosphere.

Specifically, a and b are determined by fitting the measured density profile with the relative passage altitudes reconstructed through onboard propagation. The logarithmic form simplifies this step, turning it into a linear regression. In order to desensitize the fitting process with respect to along-track errors, which can shift significantly the altitude profile, the correspondence of the density centroid and the pericentre altitude is enforced.

The prediction requires the upcoming pass a, b, and h_p values. The first two parameters can be computed by averaging those from a fixed number of previous passages, while the value of h_p can be predicted through onboard trajectory propagation. The choice of averaging for the models' free parameters determination is based on the intent of absorbing one of the major sources of atmospheric variations, i.e., those associated with solar radiation.

Another relevant aspect of atmospheric prediction concerns the execution of OCMs. Altitude changes resulting from these manoeuvres must be transmitted to the atmospheric predictor to correct the values of a and b involved in the averaging process. Whereas the parameter b is related to the scale height, which remains nearly constant

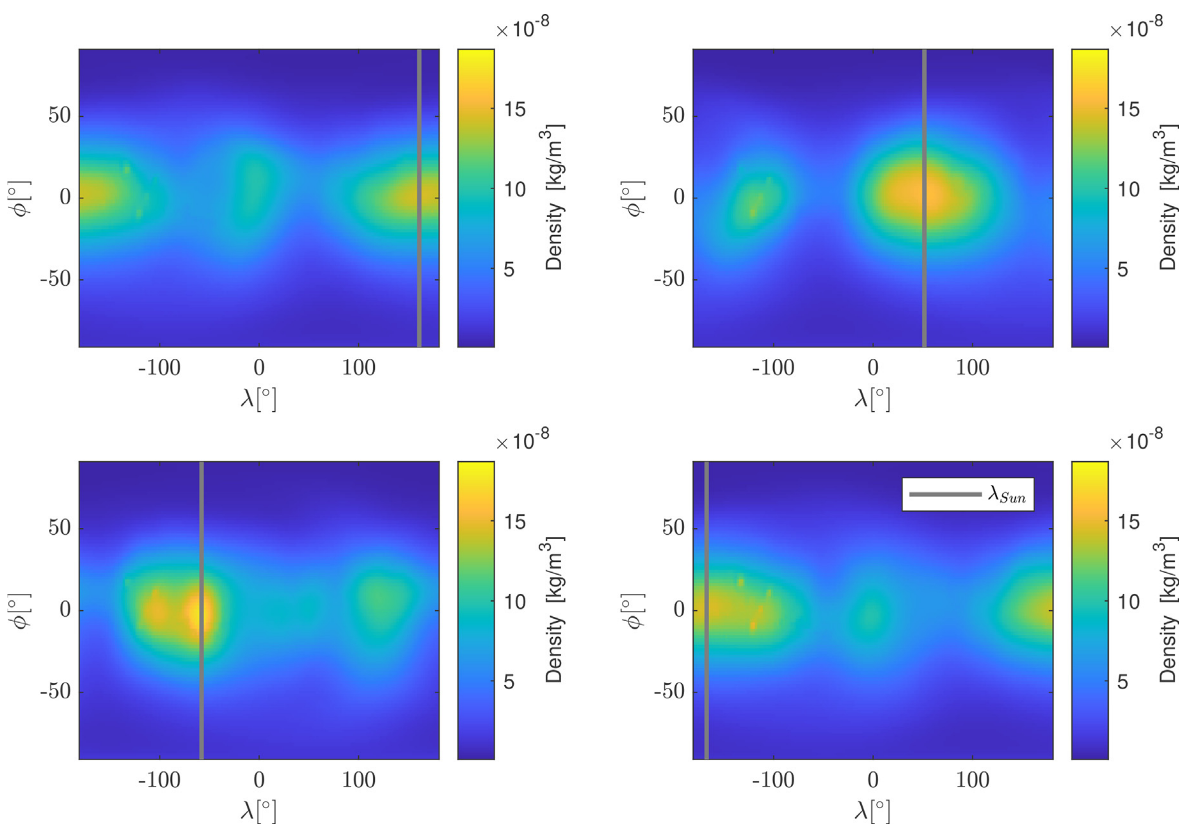

Fig. 4. Atmospheric density at a fixed altitude above Martian mean radius as function of latitude and longitude. Each map refers to a different Sun longitude in MCMF frame, represented as a solid gray line on each plot.

in the aerobraking atmospheric layers, the parameter a, associated with the pericentre density, may undergo higher variation if a high-intensity OCM is performed. Not considering this aspect can delay the effect of the manoeuvre in the atmospheric predictor, leading to cycling and consequently to wasting of fuel. Recalling from Eq. (8) that $a = \log(\rho_p), b = -\frac{1}{H}$ and that H values are stable for low h_p variations, the values of a of the passages involved in the prediction process can be updated as follows:

$$a_{updated} = a + b\ \Delta h_{man} \tag{10}$$

Eq. (10) uses the exponential relation to compute pericentre densities at an altitude equal to that of the actual pericentre plus the change in altitude Δh_{man} resulting from the OCM.

4.2. Orbital state estimation

The orbital state reconstruction is performed onboard, propagating the onboard models. This approach is preferred to the classical navigation methods that employ filtering techniques because, as shown in Hanna and Tolson (2002), propagation can provide sufficiently accurate results for aerobraking control purposes. In most cases, during aerobraking, the spacecraft does not perform science, so a high-accuracy knowledge of the orbital state is not required. A good estimate of the pericentre altitude is sufficient for OCMs execution. However, the propagation approach has some drawbacks related to the limited predictive capabilities of onboard models, which lead to a rapid dephasing of the onboard orbit with respect to the real one. To ensure the efficiency of OCMs, the along-track uncertainties must be contained. In this work, two corrections utilizing accelerometer data are performed for this purpose. The first one involves the consideration of the gap between the real drag profile a_{real} and the predicted one a_{pred}:

$$\Delta v_d = \int_{t_{in}}^{t_{out}} \left(a_{real} - a_{pred}\right) dt \tag{11}$$

The Δv_d is applied in the onboard trajectory propagation at the time corresponding to the centroid of the drag difference profile, and a multiplicative factor is considered for the transformation of the deceleration profile into an impulse. Despite this first correction, the along-track errors accumulate due to the non-perfect drag knowledge and the presence of unmodeled orbital perturbations. The dephasing of the onboard orbit can increase to the point that using the information related to the centroid of the measured drag profile is preferable. The centroid time can be computed through the data collected from the accelerometer after the passage:

$$t_{centroid} = \frac{\sum_{i=1}^{N} t_i\ a_i}{\sum_{i=1}^{N} a_i} \tag{12}$$

where a_i are the acceleration measurements, t_i the relative acquisition times, and N represents the number of measurements collected. If the time difference between the onboard trajectory pericenter and the centroid exceeds a specific threshold, the centroid time is considered more reliable, and an along-track shift of the orbit is performed according to the time difference.

Due to the differences between onboard models and real-world ones, the described corrections are not sufficient to prevent onboard trajectory degradation. Consequently, radiometric navigation is required to provide a state update. Given the stability of the pericentre altitude estimation and the aim to limit ground station involvement, a state update interval of the onboard trajectory equal to one week is considered for all simulations performed. This assumption is beneficial for a regular scheduling of aerobraking operations to be performed on ground. Note that this state update frequency is more suitable for the initial phases of aerobraking. As aerobraking progresses, smaller orbital periods can enhance the degradation of the onboard orbital state due to the increased passage duration, which amplifies the effect of uncertainties associated with atmospheric density. Adopting a conservative approach, the state update frequency is not modified throughout aerobraking execution, assuming the one-week frequency update as a worst-case scenario.

4.3. Orbit control

Orbit control can be a challenging task in the Martian environment. Besides manoeuvres optimality, the high variability must be considered in the orbit control strategies, and in fact, their development is driven by several features that encompass both aspects. Indeed, the control logics must have limited sensitivity to perturbations and responsive action to pronounced perturbative trends. Moreover, they should minimize fuel consumption and ensure the safety of the satellite. The reported drivers are in conflict, and the implemented control logics attempts to find an adequate trade-off.

4.3.1. Single Pericentre Prediction Control (SPPC)

The first implemented control logic is based on the principle presented in Maddock et al. (2012), which consists of planning and executing an OCM if a departure from the control corridor is expected at the future atmospheric passage. The intensity of the control manoeuvre is defined according to the deviation of the predicted control variable with respect to the target one. Given the high relevance of the heat rate in the Martian context, it is selected as the control variable for this control methodology.

The real maximum heat rate values experienced during the atmospheric passages are not considered to desensitize the control action with respect to temporary perturbations. This phenomenon can trigger undesired OCMs, affecting the fuel optimality of the orbit control. The manoeuvre

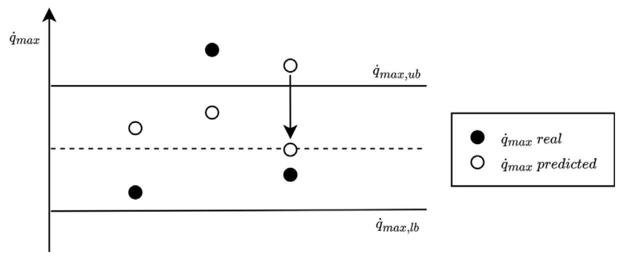

Fig. 5. SPPC logic representation.

decision-making process is based exclusively on the single future pericentre predicted heat rate. For this reason, the methodology is called Single Pericentre Prediction Control (SPPC). In Fig. 5, a graphical representation of the logic is reported.

The definition of a corridor is essential for minimizing fuel consumption as it allows for delaying and executing an OCM only if it is strictly required. The corridor centre, which represents the target heat rate value, is determined by the margins imposed on the actual satellite limits. For what concerns the width, it is selected according to a balance between responsiveness and limited sensitivity to perturbation of the control action.

The future pericentre heat rate value is determined through onboard propagation. If this value violates the corridor bounds, an OCM is planned and executed at the following apocentre, and its intensity is determined to provide a predicted heat rate coincident with the target one. In this work, the relation between the manoeuvre Δv and the difference between the desired and the predicted heat rate is retrieved analytically. Starting from the exponential model relation, under the hypothesis of small altitude variation (typical of the main phase and the end game control), using the predicted density as a reference, the generic desired density can be expressed as follows:

$$\rho_d = \rho_p \exp\left(-\frac{h_d - h_p}{H}\right) \tag{13}$$

where the subscripts d and p stand for desired and predicted respectively. Inverting Eq. (13), the change in pericenter height required to move from the predicted density to the desired one is:

$$\Delta h = -H \ \log\left(\frac{\rho_d}{\rho_p}\right) \tag{14}$$

Considering the small variation in the orbital semi-major axis associated with an OCM, the density ratio can be considered equal to the heat rate ratio. The manoeuvre Δv can be related to the semi-major axis change by means of the Gauss variational equations (Battin, 1999):

$$\Delta a \approx \frac{2a^2}{\mu} v_p \Delta v \tag{15}$$

where v_p is the pericenter velocity and μ the planet gravitational constant. Given that a variation in the pericentre altitude corresponds to half of a variation in the semi-major axis and combining Eq. (14) and Eq. (15), the impulse of pericenter height regulation to move from the predicted maximum heat rate condition to the desired one is provided by:

$$\Delta v = -H \ \frac{\mu}{4 \ a^2 \ v_p} \ \log\left(\frac{\dot{q}_d}{\dot{q}_p}\right) \tag{16}$$

where H is the scale height, μ is the planet gravitational constant, a is the orbit semi-major axis and v_p the pericentre velocity.

4.3.2. Multiple Pericentre Prediction Control (MPPC)

The broadening of the prediction horizon can provide additional information exploitable in the manoeuvre planning process. This aspect characterizes the second control logic implemented, which is called Multiple Pericentre Prediction Control (MPPC). The foundation of the methodology is based on the possibility of exploiting favorable pericentre trends to reduce fuel consumption and to make an early correction of an adverse trend, reducing aerobraking time and damping atmospheric perturbations. The sequence of operations that characterizes the MPPC can be summarized by the following points:

- Predict successive pericentre altitudes
- Centre pericentre altitudes control corridor
- Verify whether the predicted pericentre altitudes fall within acceptable limits and, if required, collocate the OCMs in the control horizon
- Optimize manoeuvres Δv

The control variable selected is the pericenter altitude. Due to the illumination conditions' evolution during aerobraking execution, it is not possible to define absolute limits for this control variable. It is crucial to consider the recent heat rate levels experienced in order to identify the trustable region in which the pericentre altitude can evolve, keeping the satellite safe. The starting point for defining the corridor's centre is the past passages' mean pericentre altitude $\bar{h}_p$. This value is then shifted proportionally to the deviation of past passages' average maximum heat rate $\bar{\dot{q}}_{max}$ from the target heat rate of the logic $\dot{q}_{target}$:

$$h_{centre} = \bar{h}_p + k \ \left(\bar{\dot{q}}_{max} - \dot{q}_{target}\right) \tag{17}$$

where k represents a proportional shift factor that regulates the responsiveness of the logic. Setting higher values of the parameter enhances the tracking of the target heat rate but also increases sensitivity to atmospheric perturbations and the OCM frequency.

The prediction horizon involves a fixed number of pericentre passes. The last known state at the time of control routines execution is propagated on-board, and the pericentre altitudes of the passes of interest are extracted. The trigger condition selected for control execution is the departure from the corridor limits of three consecutive pericentres. If the manoeuvres are triggered, the planning and magnitude computation of the OCMs is required. The scheduling principle adopted aims to avoid high-intensity manoeuvres to limit the variability of the experienced maximum heat rate. The available manoeuvres are positioned to adjust the pericentres altitudes that favor the departure from the corridor limit that triggered the control action. Fig. 6 represents the scheduling of two manoeuvres for a possible uncontrolled pericentre altitude prediction trend. Once the manoeuvres are scheduled, their magnitude is obtained solving the following problem:

$$\begin{aligned} &\underset{\Delta \boldsymbol{v}}{\text{minimize}} \sum_i |\Delta v_i| \\ &\text{subject to} \begin{cases} h_p < h_{ub} & \forall\ h_p \in P \\ h_p > h_{lb} & \forall\ h_p \in P \\ |\Delta v_i| > \Delta v_{min} \end{cases} \end{aligned} \tag{18}$$

where $\Delta \boldsymbol{v}$ is the vector of OCMs, P is the prediction horizon, h_{ub} and h_{lb} represent respectively the upper and lower bound of the altitudes corridor, and Δv_{min} is the minimum magnitude of the OCM. The optimization variables of the problem are the OCMs planned through the scheduling principle described above, and the objective function is constituted by the sum of the absolute value of their magnitude. The constraints impose a minimum manoeuvre magnitude and force the pericentres altitude of the prediction horizon to fall inside the defined corridor limits. Furthermore, the pericentres altitude nonlinear constraint enforces the execution of the OCMs at the apocentres preceding the pericentres whose altitude must be adjusted according to the planning logic used. A minimum separation of two successive manoeuvres in terms of number of revolutions can also be imposed. For all the simulations performed, two consecutive OCMs are separated by at least two revolutions, the number of pericenters of the prediction horizon has been considered equal to 6, and the value of Δv_{min} equal to 2 cm/s.

The number of states of the problem in Eq. (18) is minimized to enhance convergence through the following considerations. First, the Δv has been considered purely tangential since the other components are not functional for the desired control and, therefore, not optimal. In addition, the optimal burn time is fixed at the apocentres, where controllability of the upcoming pericentres is maximized. The problem is solved through MATLAB®'s nonlinear programming solver `fmincon`. Specifically, the sequential quadratic programming (SQP) algorithm is used. Note that this choice is compatible with MATLAB C/C++ code generation requirements for the production of embedded software to be deployed on single board computer units.

4.4. Operations sequence

The operations presented in the previous sections underlie the process of OCMs planning and execution. In Fig. 7, they are reported along with the relative information flows. The accelerometer output represents the only relevant onboard measurement extractable from the real world for orbit control purposes. This information is crucial to mitigate the degradation of the onboard trajectory with respect to the real one, allowing the limitation of the time allocated to radiometric tracking. The accelerometer measurements are used in the onboard propagator to compensate for the Δv discrepancy between the predicted and real drag experienced. Furthermore, the centroid time of the real profile is used for an along-track correction in case of excessive trajectory degradation. The data relative to the passage (altitude profile and acceleration measured) are employed to tune the onboard atmospheric predictor. Once the atmospheric model is updated, the upcoming pericentre passages data are predicted. Based on this prediction information, the orbit control block plans and executes the OCMs. The control action information is subsequently provided to the onboard propagator and used in the atmo-

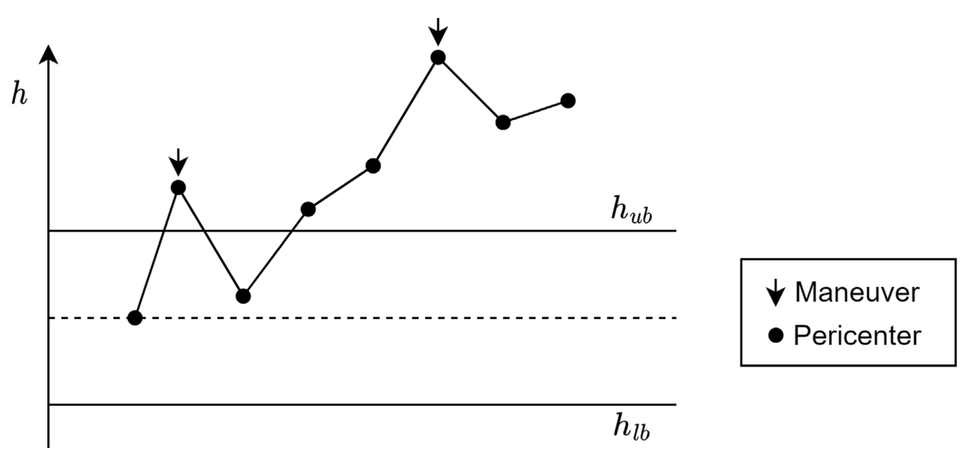

Fig. 6. OCMs collocation logic of MPPC.

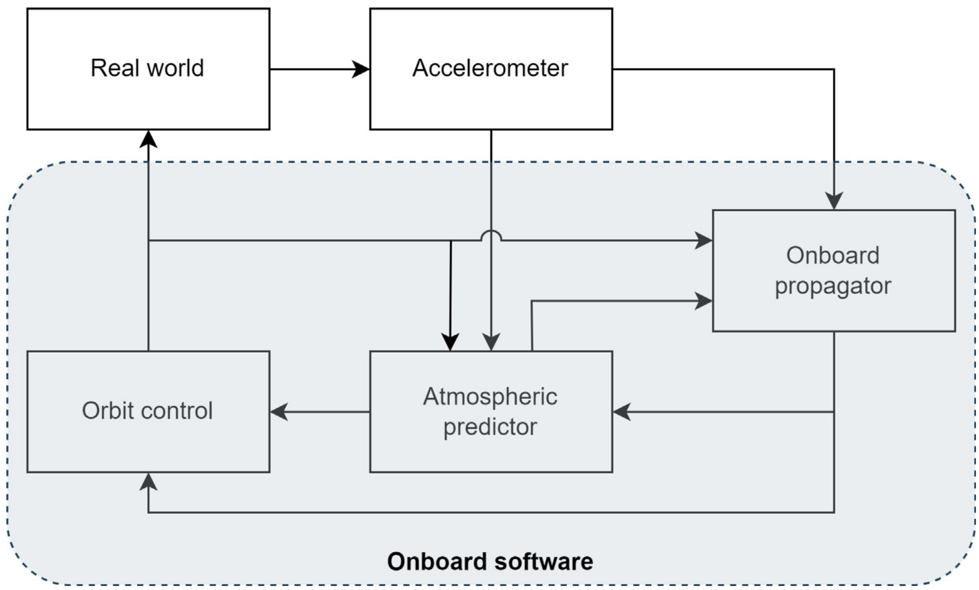

Fig. 7. Onboard operations scheme.

spheric predictor to update it according to the altitude variation induced by the control manoeuvre. The whole sequence of operations is performed once per orbit after 15 min from the time corresponding to the drag peak registered during the atmospheric passage.

5. Simulations

5.1. Testing methodology

The Martian atmospheric features have driven the testing criteria of the implemented control methodologies. The planet's topography and its interaction with solar radiation cause significant variations in atmospheric properties. Consequently, different density values and density time evolution characterize different latitudes and longitudes on Mars. Specifically, mid-latitudes exhibit more pronounced perturbations due to the significant topographic gradients. The orbital period is another crucial parameter for aerobraking operations. As shown in Fig. 3, in highly elliptical orbits, additional perturbations acquire relevance in the orbital motion and the pericentre region evolution. Furthermore, the orbital energy determines the atmospheric passage duration and the spacecraft relative velocity, which can amplify the effect of atmospheric variabilities in the operational routines.

Considering the relevance of the pericentre region and the orbital period, the following testing methodology is adopted. For starting orbital periods of 24 h, 12 h, and 6 h, the pericentre is located in the latitude interval $[-60^\circ, 60^\circ]$, equally spaced with a subinterval width of 20°. Each simulation involves 120 passages through the atmosphere to guarantee sufficient coverage of the latitude interval caused by the natural apsis precession. The pericentre longitude is not imposed since the gradual orbital period reduction allows a natural span of the atmospheric regions in terms of longitudes. In addition to the testing described above, a complete aerobraking simulation and an associated Monte Carlo analysis are performed to evaluate the control stability and robustness over an extended period. For all the simulations, the orbital inclination is considered equal to 74° according to TGO orbit at the beginning of the aerobraking phase.

5.2. Control parameters selection

As for TGO operation, the maximum heat rate tolerable by the spacecraft is considered equal to 0.28 W/cm^2. However, for the target heat rates of the implemented control methodologies, this value is margined to account for the reduced flexibility that characterizes the absence of human intervention. Furthermore, since one of the testing objectives is to highlight the differences between the two logic, the control parameters are selected to obtain a fair comparison.

Eight past passage data are considered in the fitting process of the onboard atmospheric model. The centre of the SPPC corridor is set equal to 0.075 W/cm^2, and the corridor width is equal to 0.03 W/cm^2. For the comparison reason presented above, the last eight passages are considered in the altitude and heat rate mean of the MPPC. Moreover, its corridor width is retrieved converting the SPPC density corridor to an altitude one through the exponential relation. With the typical scale height of aerobraking atmospheric layers, a value of 2 km is obtained. The target heat rate of MPPC considered is 0.1 W/cm^2. This value is higher with respect to the SPPC to account for the frequent peaks in the real density profiles that deviate from the smooth exponential profiles. Finally, the MPPC proportional shift factor k is imposed equal to 40 $km\ cm^2/W$. This value guarantees a good compromise between target heat rate tracking capability and sensibility to atmospheric perturbations. Its selection is performed empirically based on some short-term simulations.

5.3. Results

5.3.1. Short-term simulation set

The first aspect highlighted from the results is the efficiency of MPPC in terms of fuel consumption. As reported in Fig. 8, in 95% of the testing cases, the amount of Δv used by MPPC is smaller than SPPC one, and the average gain of fuel is about 60%. As expected, the most critical regions from a fuel consumption perspective correspond to the mid-latitudes, which, as anticipated in Subsection 5.1, feature higher atmospheric variabilities. However, this latitude range is sometimes exceeded by the 60° latitude. Although the latter region presents more stable atmospheric layers, it is characterized by a pronounced pericentre trend that results from the Martian gravitational anomalies and must be counteracted to satisfy mission requirements.

Interestingly, lower latitudes present lower propellant consumption. This convenience is related to the same aspect characterizing the higher latitudes. Both regions feature increasing trends of pericentre altitude dictated by the gravitational anomalies. In addition, the same orbital perturbations cause a precession of pericentre towards northern latitudes. The combination of these two phenomena underlies the different Δv consumption of the cases. For lower latitudes, while the pericentre altitude increases, the pericentre latitude moves closer to the mid-latitude range, which presents, on average, higher density values. This leads to the exploitation of the natural pericentre evolution. In the case of higher latitudes, the orbit control cannot benefit from the natural motion as the pericentre moves toward more rarefied atmospheric layers. Therefore, OCMs are required not only to counteract the trend but also to reduce the pericentre height to avoid the violation of the control corridor lower bound. Fig. 9 represents the aforementioned trends for the simulation cases associated with the highest and the lowest Δv consumption when control is performed through the MPPC methodology.

Another notable aspect of Fig. 8 regards the concentration of high fuel consumption test cases in the lower starting orbital period. This trend is mainly related to the decrease in efficiency that OCMs undergo; for lower apocentre altitudes, more fuel is required to obtain the same pericentre altitude variation.

Besides the higher Δv efficiency, the MPPC reveals enhanced perturbation damping capabilities with respect to SPPC. This aspect can be grasped from Fig. 10, where the standard deviation of the experienced heat rate is reported for each test case. Once again, $[-20^\circ, 20^\circ]$ latitude range presents higher variabilities, which are even more pronounced when orbit control is performed through SPPC methodology. Although this last logic shows better performances for some starting latitudes, MPPC always outperforms it in the most critical cases, i.e., mid-latitudes. Note that the perturbation damping property is essential in aerobraking execution for safety reasons and operational cost reduction since it allows to relax margins and, consequently, to perform faster aerobraking manoeuvres.

5.3.2. Complete aerobraking simulation

The target heat rates defined in Subsection 5.2 are increased for the complete aerobraking simulation since none of the previous testing cases reported a violation of the heat rate limit; rather, they revealed sufficient margin. MPPC target is raised to 0.13 W/cm^2 and SPPC one to 0.105 W/cm^2. As for the short-term simulation set, the difference between the target heat rates of the two control strategies is required to compensate for the peaks that the actual heat rate profile (used in the MPPC strategy) features with respect to the smooth profiles obtained through

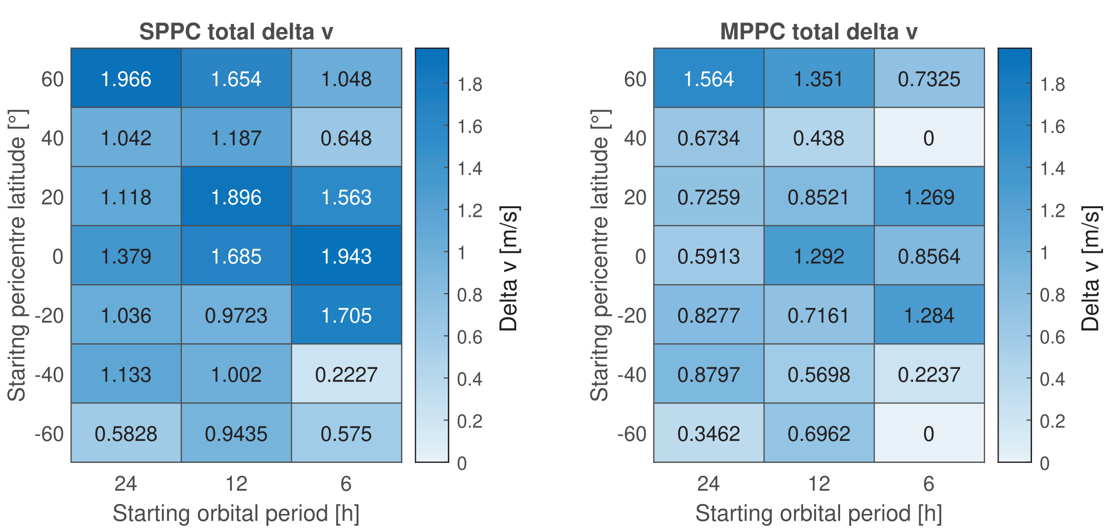

Fig. 8. Total OCMs fuel consumption for each test case.

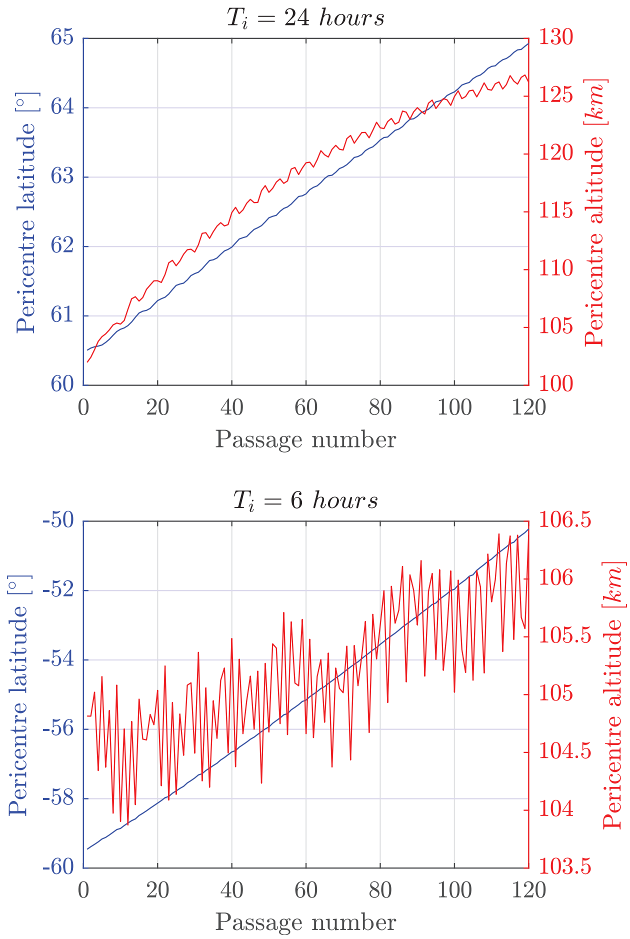

Fig. 9. Uncontrolled pericentre latitude and altitude trend for the simulation cases associated with a starting pericentre latitude of 60° and orbital period of 24 h (top figure), and starting pericentre latitude of −60° and orbital period of 6 h (bottom figure).

the onboard exponential model, which is the foundation of the SPPC OCMs scheduling process. All the other parameters have remained unchanged. The starting latitude is set equal to −40°, and the starting and exiting orbital periods are the ones of the TGO aerobraking campaign (Table 1). No solar conjunctions are considered in the simulation and the state update from radiometric navigation, when required, is considered always available. Fig. 11 reports the heat rate trends for uncontrolled aerobraking, controlled through SPPC and MPPC.

In the uncontrolled case, a considerable heat rate limit violation is registered, followed by a significant reduction that almost jeopardizes the conclusion of the aerobraking manoeuvre. Instead, the two control methodologies succeed in ensuring the proper and safe execution of the manoeuvre. Table 2 reports the most relevant parameters of the three simulations. Similar conclusions to the previous test cases can be drawn. The MPPC efficiency in terms of propellant consumption emerges, as well as its enhanced perturbation damping capability. The improved perturbation handling can be noticed from the reduced dispersion in the maximum heat rate experienced during the atmospheric passage, as shown in Fig. 11. This improvement also emerges from the lower maximum heat rate reported in Table 2, despite the methodologies revealing similar mean maximum heat rates. Furthermore, MPPC demonstrates a satisfactory performance concluding the aerobraking with an average heat rate $\bar{\dot{q}}_{max}$ that deviates from the target value of about 6%.

In Fig. 12, the heat load experienced during aerobraking executed with the SPPC is presented. As anticipated in Subsection 4.3.1, the heat rate represents the most relevant control parameter for aerobraking at Mars since it constitutes the most stringent constraint. However, a rapid heat

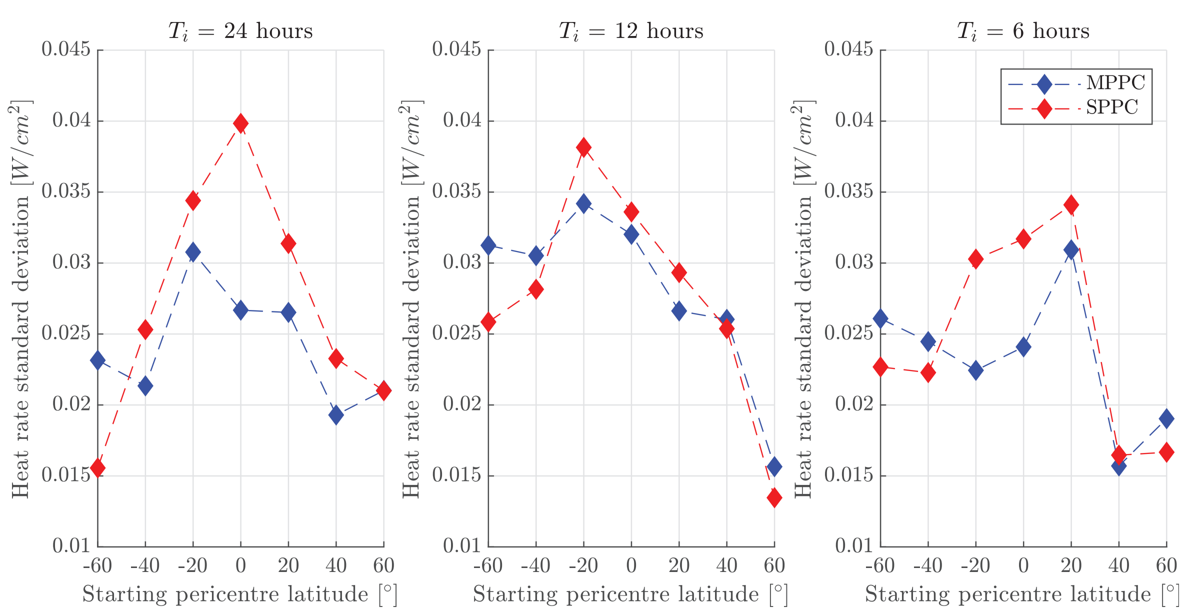

Fig. 10. Standard deviation of the maximum heat rate experienced during atmospheric passages of each test case.

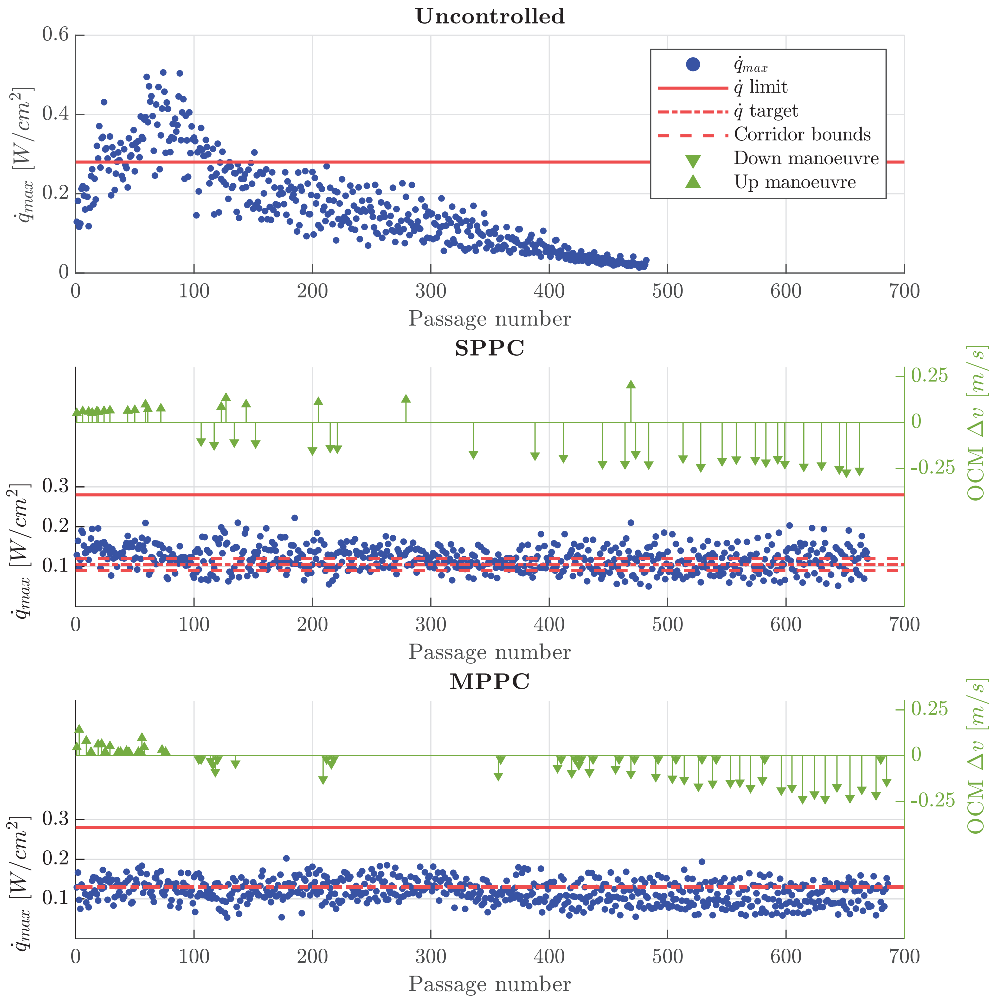

Fig. 11. Maximum heat rate experienced for an uncontrolled aerobraking, controlled with SPPC and controlled with MPPC.

Table 2
Relevant parameters of the complete aerobraking simulation.

	Δv_m $\left[\frac{m}{s}\right]$	t_{el} $[d]$	$\bar{\dot{q}}_{max}$ $\left[\frac{W}{cm^2}\right]$	$\dot{q}_{max}$ $\left[\frac{W}{cm^2}\right]$	n_m $[-]$
Uncontrolled	0	111.6	0.176	0.508	0
SPPC	6.81	199.4	0.124	0.223	46
MPPC	5.43	205.2	0.122	0.202	68

load increase characterizes the last passages of the aerobraking, suggesting the consideration of this parameter for future developments of the implemented control methodologies.

The trajectory followed during the whole aerobraking campaign is represented in Fig. 13. Note that the apocentre decreasing rate is higher for more elliptical orbits as the Δv depleted from the atmospheric passes is more efficient at the initial aerobraking phases. Furthermore, orbit orientation variations are more marked for lower orbits due to the increased influence of the Martian gravitational perturbations.

In order to assess the robustness of the control strategies, a Monte Carlo analysis has been carried out on the complete aerobraking simulation. The analysis considered

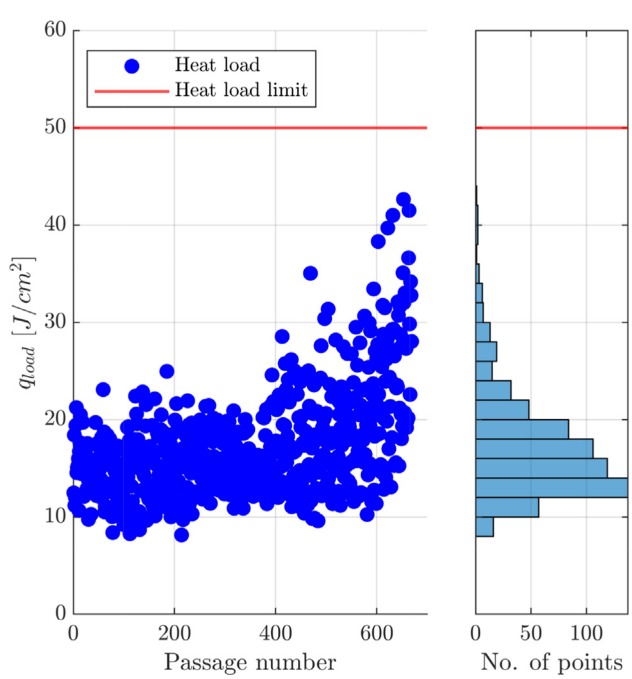

Fig. 12. Heat load trend during aerobraking controlled through SPPC.

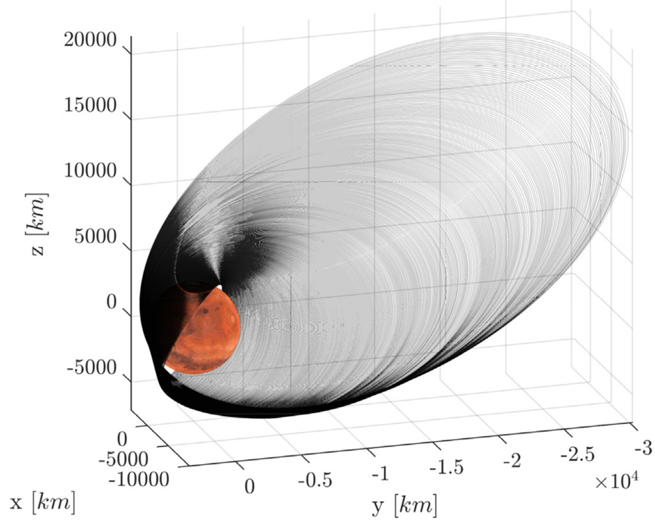

Fig. 13. Orbital trajectory of aerobraking controlled through SPPC in J2000 reference frame.

a set of 50 samples with perturbed initial orbital state and drag coefficient. Specifically, the initial position and velocity have been sampled uniformly from a sphere with a diameter of 5 km and 2 cm/s^2, respectively. The C_d has been sampled uniformly from the range $[-10\% + 10\%]$ of its nominal value. In Fig. 14, the results of the simulations are presented in terms of total Δv consumption, number of OCMs performed, variance of the maximum heat rate experienced, and total aerobraking time.

Neither control logic reported thermal violations throughout the simulations, highlighting their stability over an extended period of time and robustness under non-nominal conditions. The results obtained are coherent with the ones of the first simulation set; the Monte Carlo analysis demonstrates a higher efficiency of the MPPC in terms of total fuel consumption. The SPPC reveals, on average, 25.5% more Δv consumption than the MPPC. While still a significant difference, it can be noted that it is not comparable with the 60% obtained in the short-term simulations. This difference is related to the pericentre altitude trends, which require a similar delta-v for the two strategies. Acting for a longer time span in the complete aerobraking simulations, they flatten out the differences in fuel consumption.

The second parameter that features a significant discrepancy is the number of OCMs performed. The MPPC uses, on average, 56.6% more OCMs with respect to the SPPC in the complete aerobraking simulations, a value coherent with the 78.5% increase of the short-term simulations set. The higher number of manoeuvres required by the MPPC is related to how the OCMs scheduling process of the strategy behaves when pronounced pericentre trends are experienced and will be explained more in detail in Subsection 5.3.3.

The last quantities reported in Fig. 14 are the heat rate variability and the total aerobraking time. Both control logics required comparable aerobraking times, with a difference of just 1.9 days. This similarity is the outcome of the control parameter selection, which aims to ensure a fair comparison of the two methodologies. In this study, aerobraking time is considered a meaningless figure of merit for the analysis due to its sensitivity to high heat rates, which can result from a control logic that does not correctly handle atmospheric perturbations. Therefore, it is used only as an indicator of comparison fairness. In addition to aerobraking time, the other parameter representative of the fact that during the simulations the two control logics have operated under similar conditions is the mean maximum heat rate. The average value of 0.1233 W/cm^2 for the SPPC and 0.1231 W/cm^2 for the MPPC further support the fairness of the comparison.

Given that comparison purposes constrain the total aerobraking time, it is not possible to unequivocally state which of the strategies enables faster aerobraking. How-

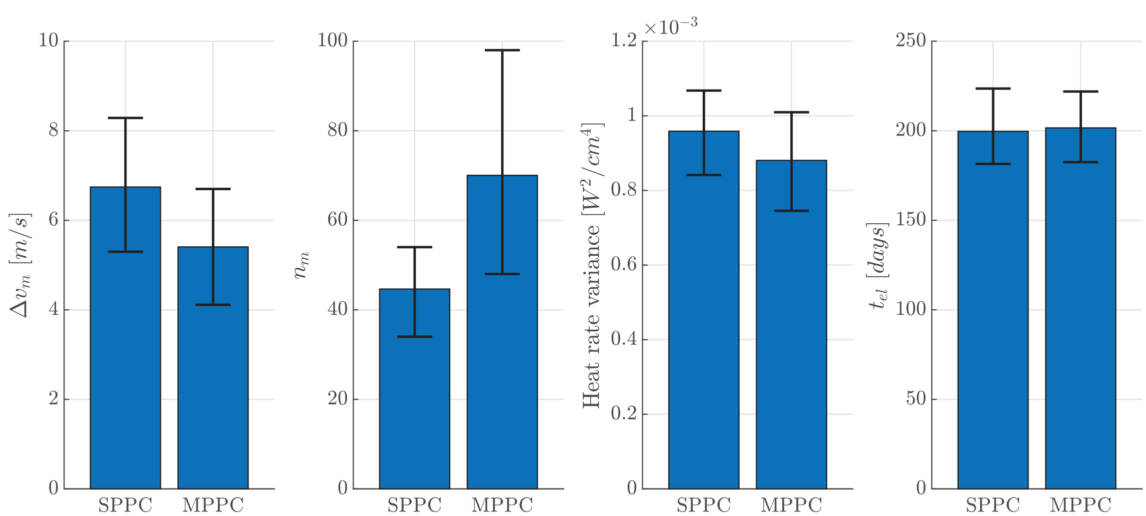

Fig. 14. Comparison of total delta v consumption, number of OCMs performed, heat rate variance, and total aerobraking time for the Monte Carlo analysis. The bar value represent the mean and the bands are the range of values that the specific quantities covered during the simulations.

ever, considering the heat rate variance reported in Fig. 14, some conclusions regarding aerobraking performance can be drawn. The parameter presents a 9.4% increase for SPPC simulations compared to the MPPC ones. The lower heat rate variance of the MPPC can potentially be translated into improved performance. Advantages involve safety since the limited heat rate variability leads to more stable conditions during flight and also aerobraking time, considering that a higher target heat rate could be used during aerobraking execution. Furthermore, the more stable conditions can be beneficial in mission scenarios where specific semi-major axis trends are imposed by mission constraints.

5.3.3. Comparison and considerations

The simulation results highlighted as the main differences between the two methodologies involve fuel consumption, number of OCMs performed, and capability to handle perturbations. The reasons underling this differences will be explained by considering two cases of the short-term simulation set. The first simulation considered is the one relative to a starting pericentre latitude of -20° and a starting orbital period of 12 h. Fig. 15 represents the maximum heat rates experienced along with the corresponding pericentre altitude profiles followed during the atmospheric passages, respectively for the SPPC and the MPPC. This simulation is useful to explain the advantage of using MPPC over SPPC. Considering the range of passages between 1 and 20, it can be noted that SPPC triggers a down manoeuvre while MPPC does not. This aspect is related to the limited predictive horizon that characterizes the SPPC. Specifically, high initial heat rates trigger more up manoeuvres regardless of the following natural upward trend of the pericentre that characterizes the following passages. Due to this trend, the multiple up OCMs of the SPPC result in excessive control action that triggers a down manoeuvre to compensate. On the other hand, the broader prediction horizon of the MPPC captures the trend and, through its exploitation, avoids a larger overall up manoeuvre, preventing the subsequent triggering of a down manoeuvre. The same situation occurs in the proximity of passage number 100. Even in this case, an increase in heat rate is followed by a rising trend of the pericentre altitude, which is exploited by the MPPC but not by the SPPC. The latter performs an up manoeuvre followed immediately by a down manoeuvre to compensate for the non-optimal action performed.

The highlighted aspects underlie the lower fuel consumption and the reduced maximum heat rate variability that characterizes the MPPC, whose advantages are based on its ability to exploit short-term pericentre trends. MPPC limitation emerges when such trends are marked and sustained over time. Fig. 16 represents the simulation associated with a starting orbital period of 24 h and starting pericentre latitude of -40°, characterized by a pronounced decreasing pericentre trend. As for the previous case, the

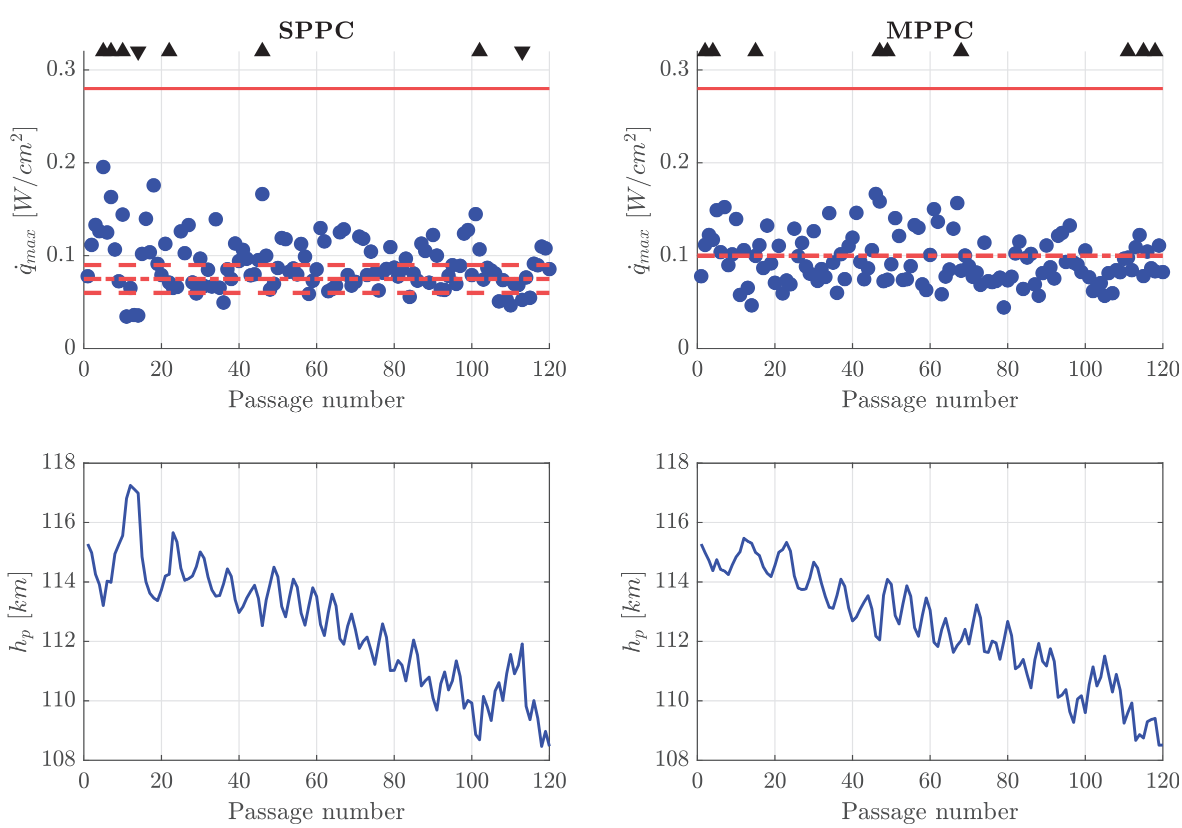

Fig. 15. Maximum heat rate and pericentre altitude trend for starting orbital period of 12 h and starting pericentre latitude of -20°.

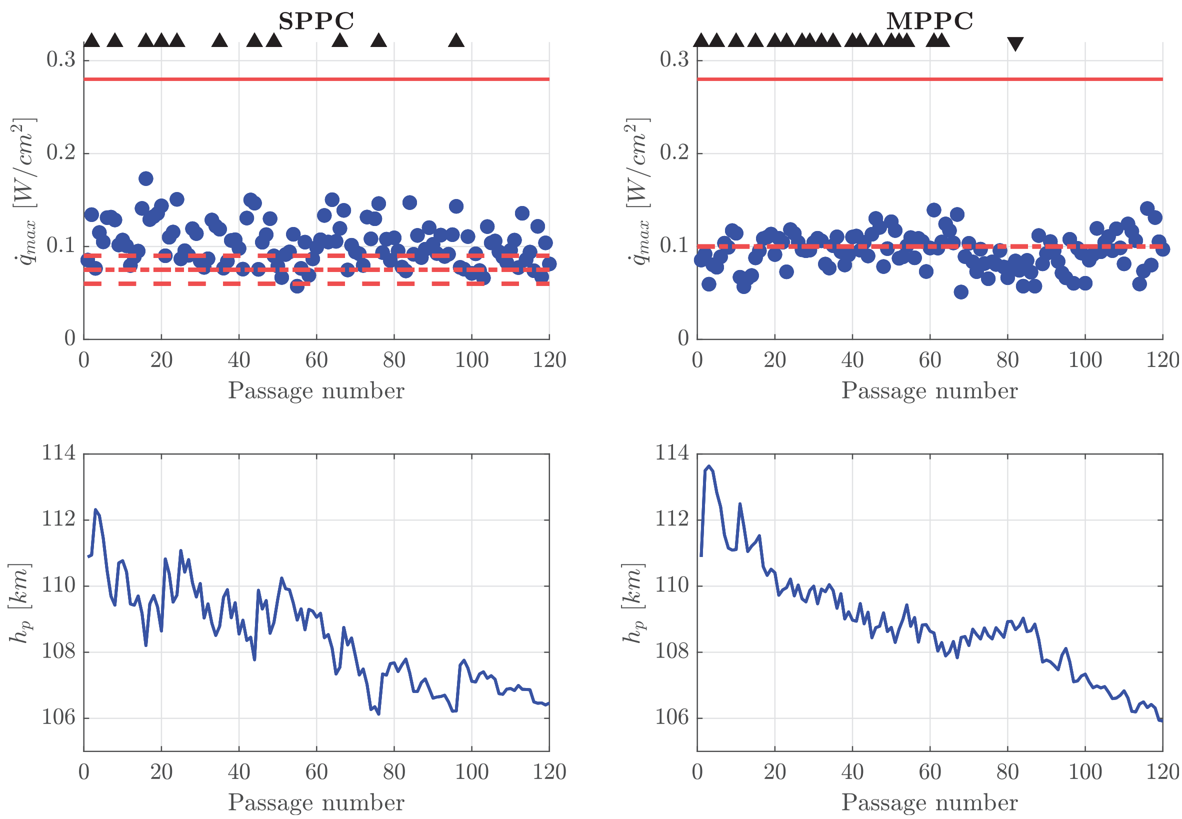

Fig. 16. Maximum heat rate and pericenter attitude trend for starting orbital regime of 24 h and starting pericenter latitude of −40°.

experienced heat rates and the pericentre altitudes relative to each atmospheric passage are represented. It can be noticed that the pronounced trend leads the MPPC to the planning of multiple raising OCMs in short periods of time, while the SPPC achieves similar results with a reduced number of manoeuvres, resulting in the optimal method in this case. Depending on the inertial characteristics of the satellite and the need for ground communication, a high number of OCMs may be problematic due to the increased number of slews required to reach the OCM attitude. Despite the lower optimality, even in this case, the perturbation handle capability of the MPPC emerges from the more contained variability in the maximum heat rates registered, resulting from a more controlled descent.

6. Conclusions

This work investigates possible solutions for planning and executing OCMs required by aerobraking's main phase and end game. The focus is placed on reducing ground resource utilization and leveraging information available onboard to enhance autonomy. The implemented aerobraking operational loop, which consists of atmospheric prediction, orbital state reconstruction, and orbit control, is numerically tested in a real-world model representative of the Martian environment. In this context, emphasis is devoted to the high-fidelity reproduction of the atmospheric variability that characterizes the atmospheric layers involved in aerobraking passages. For this purpose, the MCD is employed to provide the atmospheric density values during orbital motion propagation.

Given the limited fidelity of onboard resources, the onboard accelerometer represents an essential element functional to the mitigation of aerobraking operational cost; accelerometer measurements are employed in the characterization of atmospheric conditions, which is paramount for atmospheric prediction, and in the onboard orbital propagation, aiming at the relaxation of radiometric navigation coverage.

Concerning orbit control, two methodologies are implemented. The SPPC plans and executes OCMs according to the future pericentre predicted maximum heat rate, while the MPPC controls the altitude trend of multiple pericentre based on the maximum heat rate experienced. In order to assess their performance, the control logics are tested under different orbital regimes, atmospheric regions, and non-nominal conditions. In all the simulations, the control logics allowed aerobraking execution without thermal violations, proving their effectiveness. Furthermore, a Monte Carlo analysis performed on a complete aerobraking simulation demonstrated that MPPC reduces propellant consumption by 25.5% and decreases heat rate variability by 9.4% compared to the SPPC, which, however, uses fewer OCMs. Specifically, the results revealed an increase of 56.6% in the number of OCMs when the orbit control is performed through MPPC. The following observations can explain the differences between the two control strategies. Firstly, broadening the prediction horizon in OCM planning enables the exploitation of future pericentre trends, enhancing fuel efficiency. Furthermore, it fosters heat rate stability, preventing abrupt changes in pericentre altitude. Secondly, in case of pronounced pericentre trends, OCMs execution based on the single future pericentre condition is optimal due to the prolonged unidirectional control action required.

Although the implemented solutions provide promising results, further testing and improvements are foreseen to assess the suitability of the methodologies for an actual on-board implementation. Furthermore, the relaxation of the made assumption is needed to evaluate the possibility of using the control logics in flight. This aspect represents the foundation of possible future developments, which should increase the simulation fidelity. The most important advancements concern the transition to a 6-dof simulation, the enhancement of aerodynamic modeling to accurately reproduce the satellite's heat fluxes and side forces, and a robustness analysis on OCMs execution. An essential step forward consists of implementing a processor in the loop simulation environment, which would allow testing on relevant hardware and optimizing the algorithms according to the requirements imposed by the limited resources of on-board computers. Other efforts should be devoted to the introduction of orbit determination in the operational loop and the integration of collision avoidance strategies. Finally, further studies are required to enhance the atmospheric prediction capabilities, which represent the major current bottleneck of aerobraking. The missions heritage demonstrates that even complex models provide poor prediction results due to the reduced frequency of atmospheric passages during the manoeuvre. The ideal solution would be in situ atmospheric monitoring, which would definitively actualize the potentialities of aerobraking, making it safer and faster.

Declaration of Competing Interest

The authors declare that they have no known competing financial interests or personal relationships that could have appeared to influence the work reported in this paper.

References

Battin, R.H., 1999. Variation of parameters. In: An Introduction to the Mathematics and Methods of Astrodynamics, Revised Edition chapter 10. (pp. 471–514). doi:10.2514/5.9781600861543.0471.0514.

Castellini, F., Bellei, G., Godard, B., 2019. Mars Aerobraking Operations for ExoMars TGO: A Flight Dynamics Perspective. In: Pasquier, H., Cruzen, C.A., Schmidhuber, M., Lee, Y.H. (Eds.), Space Operations: Inspiring Humankind's Future. Springer International Publishing, Cham, CH, pp. 661–694. https://doi.org/10.1007/978-3-030-11536-4_26.

de Oliveira, M.R., Gil, P.J., Ghail, R., 2018. A novel orbiter mission concept for venus with the EnVision proposal. Acta Astronaut. 148, 260–267. https://doi.org/10.1016/j.actaastro.2018.05.012.

Demcak, S., Young, B., Graat, E. et al., 2020. Navigation Design and Operations of MAVEN aerobraking. In: AIAA Scitech 2020 Forum. doi:10.2514/6.2020-0471 AIAA 2020-0471.

Denis, M., Schmitz, P., Sangiorgi, S. et al., 2018. Thousand Times Through the Atmosphere of Mars: Aerobraking the ExoMars Trace Gas Orbiter. In: 2018 SpaceOps Conference. doi:10.2514/6.2018-2713 AIAA 2018-2713.

Falcone, G., Putnam, Z., 2019. Aerobraking Trajectory Control Using Articulated Solar Panels. In: 2019 AAS/AIAA Astrodynamics Specialist Conference. AAS Paper 19–682.

Falcone, G., Putnam, Z.R., 2023. Autonomous decision-making for aerobraking via parallel randomized deep reinforcement learning. IEEE Trans. Aerosp. Electron. Syst. 59 (3), 3055–3070. https://doi.org/10.1109/TAES.2022.3221697.

Forget, F., Hourdin, F., Fournier, R., et al., 1999. Improved general circulation models of the Martian atmosphere from the surface to above 80 km. J. Geophys. Res.: Planets 104 (E10), 24155–24175. https://doi.org/10.1029/1999JE001025.

Han, D., Young, B., 2019. Aerobraking the Exomars TGO: the JPL Navigation Experience. In: 27th International Symposium on Space Flight Dynamics 2019 (ISSFD) at 18th Australian Aerospace Congress. URL: https://hdl.handle.net/2014/50471.

Hanna, J.L., Tolson, R., 2002. Approaches to autonomous aerobraking at Mars. J. Astronaut. Sci. 50, 173–189. https://doi.org/10.1007/BF03546261.

Jah, M.K., Lisano, M.E., Born, G.H., et al., 2008. Mars aerobraking spacecraft state estimation by processing inertial measurement unit data. J. Guid., Control, Dynam. 31 (6), 1802–1812. https://doi.org/10.2514/1.24304.

Johnson, M.A., Willcockson, W.H., 2003. Mars odyssey aerobraking: the first step towards autonomous aerobraking operations. In: 2003 IEEE Aerospace Conference Proceedings (Cat. No. 03TH8652) (pp. 8_3503–8_3510). IEEE volume 8. doi:10.1109/AERO.2003.1235536.

Jones, D., Lam, T., Trawny, N. et al., 2015. Using Onboard Telemetry for MAVEN Orbit Determination. In: AAS/AIAA Space Flight Mechanics Meeting (pp. 15–202). AAS Paper 15–202.

Konopliv, A.S., Park, R.S., Folkner, W.M., 2016. An improved JPL Mars gravity field and orientation from Mars orbiter and lander tracking data. Icarus 274, 253–260. https://doi.org/10.1016/j.icarus.2016. 02.052.

Konopliv, A.S., Yoder, C.F., Standish, E.M., et al., 2006. A global solution for the Mars static and seasonal gravity, Mars orientation, Phobos and Deimos masses, and Mars ephemeris. Icarus 182 (1), 23–50. https://doi.org/10.1016/j.icarus.2005.12.025.

Liu, G., England, S., Lillis, R.J., et al., 2017. Longitudinal structures in Mars' upper atmosphere as observed by MAVEN/NGIMS. J. Geophys. Res.: Space Phys. 122 (1), 1258–1268. https://doi.org/10.1002/2016JA023455.

Long, S., You, T.-H., Halsell, C. et al. (2008). Mars reconnaissance orbiter aerobraking navigation operation. In: SpaceOps 2008 Conference, p. 3349. doi:10.2514/6.2008-3349 paper AIAA 2008-3349.

Lyons, D.T., Beerer, J.G., Esposito, P., et al., 1999. Mars global surveyor: aerobraking mission overview. J. Spacecr. Rock. 36 (3), 307–313. https://doi.org/10.2514/2.3472.

Lyons, D.T., Saunders, R., Griffith, D.G., 1995. The Magellan Venus mapping mission: aerobraking operations. Acta Astronaut. 35 (9), 669–676. https://doi.org/10.1016/0094-5765(95)00032-U, Challenges of Space for a Better World.

Maddock, R., Bowes, A., Powell, R., et al., 2012. Autonomous Aerobraking Development Software: Phase One Performance Analysis at Mars, Venus, and Titan. AIAA/AAS Astrodynamics Specialist Conference. https://doi.org/10.2514/6.2012-5074, paper AIAA 2012-5074.

Millour, E., Forget, F., Lewis, S., 2017. Mars Climate Database v. 5.3. User Manual.

Montenbruck, O., Gill, E., 2000. Satellite Orbits: models, methods, and applications. Springer, Berlin Heidelberg. https://doi.org/10.1007/978-3-642-58351-3.

Moudden, Y., Forbes, J., 2008. Topographic connections with density waves in Mars' aerobraking regime. J. Geophys. Res.: Planets 113 (E11). https://doi.org/10.1029/2008JE003107.

Moudden, Y., Forbes, J., 2010. A new interpretation of Mars aerobraking variability: Planetary wave-tide interactions. J. Geophys. Res.: Planets 115 (E9). https://doi.org/10.1029/2009JE003542.

Moudden, Y., Forbes, J., 2015. Density prediction in Mars' aerobraking region. Space Weather 13 (1), 86–96. https://doi.org/10.1002/2014SW001121.

Prince, J.L., Dec, J.A., Tolson, R.H., 2009. Autonomous aerobraking using thermal response surface analysis. J. Spacecr. Rock. 46 (2), 292–298. https://doi.org/10.2514/1.32793.

Rogers, R.M., 2003. Applied Mathematics in Integrated Navigation Systems volume 1. AIAA. https://doi.org/10.2514/4.861598.

Smith Jr, J.C., Bell, J.L., 2005. 2001 Mars Odyssey Aerobraking. J. Spacecr. Rock. 42 (3), 406–415. https://doi.org/10.2514/1.15213.

Spencer, D.A., Tolson, R., 2007. Aerobraking cost and risk decisions. J. Spacecr. Rock. 44 (6), 1285–1293. https://doi.org/10.2514/1.24303.

Spilker, T.R., Adler, M., Arora, N., et al., 2019. Qualitative assessment of aerocapture and applications to future missions. J. Spacecr. Rock. 56 (2), 536–545. https://doi.org/10.2514/1.A34056.

Tolson, R., Bemis, E., Hough, S., et al., 2008. Atmospheric modeling using accelerometer data during mars reconnaissance orbiter aerobraking operations. J. Spacecr. Rock. 45 (3), 511–518. https://doi.org/10.2514/1.34301.

Tolson, R., Dwyer, A., Hanna, J., et al., 2005. Application of accelerometer data to Mars Odyssey aerobraking and atmospheric modeling. J. Spacecr. Rock. 42 (3), 435–443. https://doi.org/10.2514/1.15173.

Tolson, R., Keating, G., Cancro, G., et al., 1999. Application of accelerometer data to Mars global surveyor aerobraking operations. J. Spacecr. Rock. 36 (3), 323–329. https://doi.org/10.2514/2.3474.

Tolson, R.H., Prince, J.L., 2011. Onboard atmospheric modeling and prediction for autonomous aerobraking missions. In: 2011 AAS/AIAA Astrodynamics Specialist Conference NF1676L-13164. Paper AAS 11–477.

Val Serra, S., Bonnamy, O., Witasse, O., et al., 2011. Venus express aerobraking. IFAC Proc. Vol. 44 (1), 715–720. https://doi.org/10.3182/20110828-6-IT-1002.02433, 18th IFAC World Congress.

Vallado, D.A., 2001. Fundamentals of Astrodynamics and Applications, volume 12. Springer Science & Business Media.

Walberg, G.D., 1985. A survey of aeroassisted orbit transfer. J. Spacecr. Rock. 22 (1), 3–18. https://doi.org/10.2514/3.25704.

Young, B., 2018. Practical orbit determination for aerobraking with accumulated accelerometer data. AAS John L. Junkins Dynamical Systems Symposium.

Zurek, R.W., Smrekar, S.E., 2007. An overview of the Mars Reconnaissance Orbiter (MRO) science mission. J. Geophys. Res.: Planets 112 (E5). https://doi.org/10.1029/2006JE002701.